Applied Catalysis A, General 643 (2022) 118725

Contents lists available at ScienceDirect

Applied Catalysis A, General

journal homepage: www.elsevier.com/locate/apcata

Reversible ionic liquids (RevILs) for the preparation of thermally stable SBA-15 supported gold nanoparticle catalysts

Zengran Sun [a], Ellis Hammond-Pereira [a], Xianghui Zhang [a,b], Di Wu [a,b,c,d], Steven R. Saunders [a,c,*,1]

[a] The Gene and Linda Voiland School of Chemical Engineering and Bioengineering, Washington State University, Pullman, WA 99164, United States
[b] Alexandra Navrotsky Institute for Experimental Thermodynamics, Washington State University, Pullman, WA 99164, United States
[c] Department of Chemistry, Washington State University, Pullman, WA 99164, United States
[d] Materials Science and Engineering, Washington State University, Pullman, WA 99164, United States

ARTICLE INFO

Keywords:
Switchable nature of reversible ionic liquids
Gold nanoparticles
SBA-15 mesoporous silica
Thermal stability

ABSTRACT

Reversible ionic liquids (RevILs) are ionic liquids that can be switched between molecular and ionic forms via two stimuli, and they can assist in the synthesis of colloidal gold nanoparticles. The RevIL-stabilized gold nanoparticles are deposited in the pores of SBA-15 mesoporous silica via incipient wetness without the functionalization of the SBA-15 surface. The location of nanoparticles inside the pores was confirmed by transmission electron microscopy technique and by a measured increase in the thermal stability of the nanoparticles in SBA-15 compared to non-porous silica. The porous gold catalysts are active in the selective oxidation of benzyl alcohol without calcination due to the absence of the ligands on the gold surface after deposition. Additionally, they are more active than the non-porous gold catalysts, indicating that the pore geometry enhances catalytic performance. Ultimately, the catalysts prepared by RevIL technique are thermally stable and active and show fine control over particle size.

1. Introduction

The modern catalyst design approach aims to prepare catalysts with dual functionalities: the highly active surface of metallic nanoparticles with the beneficial in-pore orientation and confinement effects afforded by high-surface area mesoporous silica [1–3]. Mesoporous silica contained metallic nanoparticle catalysts are commonly prepared by: 1. incorporating nanoparticles before the growth of pores (this leads to potential mass transport issues due to blocked pores) [4], 2. synthesizing nanoparticles within the pores [5], or 3. depositing nanoparticles inside the pores. However, all of these methods require surface modification of mesoporous silica to tether the nanoparticles (or their precursors) then necessitates calcination that leads to the deterioration of the nanoparticle morphology before the catalyst is even used [3,6–8].

Reversible Ionic Liquids (RevILs) have been shown to facilitate the preparation of SiO_2-supported gold nanoparticle catalysts by eliminating the need for calcination [9–11]. RevILs are ionic liquids that can be switched between a molecular (or non-ionic form) and ionic form via two different stimuli. RevILs are formed from a reaction of silylamine molecular liquids (e.g., 3-aminopropyltriehtylsilane, APTES) with CO_2, which forms an ammonium−carbamate ion pair (Scheme 1). Upon removal of CO_2 (via sparging with an inert or gentle heating), RevILs reverse to APTES molecular liquids. RevILs facilitate the preparation and deposition of surface-clean nanoparticles onto the surface of non-porous SiO_2 [9,10]. Additionally, RevILs have been shown to lessen the extent of sintering of nanoparticles during calcination compared to traditional thiol ligands [10]. However, the nanoparticles supported on a surface have facile pathways for particle migration and coalescence (PMC) or Ostwald ripening (OR) [12], inevitably increasing the occurrence of sintering during use or calcination. These catalysts could theoretically be further improved by replacing the non-porous silica with that of a structured, mesoporous silica. The pore geometry of mesoporous supports (e.g., SBA-15) can create geometric barriers to inhibit the sintering of nanoparticles [13].

Abbreviations: RevIL, Reversible ionic liquid; APTES, 3-aminopropyltriethylsilane; A.S., as-synthesized.

* Corresponding author at: The Gene and Linda Voiland School of Chemical Engineering and Bioengineering, Washington State University, Pullman, WA 99164, United States.
E-mail address: steven.r.saunders@wsu.edu (S.R. Saunders).
[1] http://orcid.org/0000-0001-6714-7435.

https://doi.org/10.1016/j.apcata.2022.118725
Received 23 February 2022; Received in revised form 6 June 2022; Accepted 8 June 2022
Available online 12 June 2022

An SBA-15 mesoporous silica is an ideal candidate-host for metallic nanoparticles due to its large surface area and pore volume, adjustable pore size, and various morphology [14]. Traditionally, SBA-15 supported gold nanoparticle catalysts are prepared in one of two methods: nucleation and growth of the nanoparticles within the pores or depositing prepared nanoparticles in the pores [15]. Both methods require the functionalization of the SBA-15 surface with aminosilanes before nanoparticle synthesis or deposition, where the terminal amines bind to the tetrachloroaurate ions ($AuCl_4^{-1}$) or the already-prepared nanoparticles [16–18]. Calcination removes the aminosilanes for catalyst activation [19]. Functionalizing the SBA-15 surface is time-consuming and creates potential mass-transport barriers [17,20,21]. Calcination often does not fully remove the ligands and results in the sintering of nanoparticles [22]. Furthermore, the gold nanoparticle catalysts prepared with traditional methods have a large particle size (> 30 nm), poor dispersion, or wide size distribution [23–26].

Herein, we demonstrate an improved SBA-15 supported gold nanoparticle catalyst preparation—the RevIL-stabilized gold nanoparticles are deposited in the prepared SBA-15 mesoporous silica via an incipient wetness (IW) technique, leveraging the switchable nature of RevILs. This will provide two clear improvements compared to traditional methods: 1. removing the need to modify the mesoporous silica surface, and 2. eliminating the need for calcination, thus improving the control over nanoparticle size.

2. Materials and methods

2.1. Materials

Gold (III) chloride trihydrate ($HAuCl_4 0.3H_2O$; ≥ 99.9 % trace metal basis), allylamine ($C_3H_5NH_2$; 98 %), hydrochloric acid (HCl; 37 %; ACS Reagent), poly(ethylene glycol) -block-poly(propylene glycol)-block-poly(ethylene glycol) (P123, $C_3H_3O[C_2H_4O]x[C_3H_6O]y[C_2H_4O]zC_3H_3O_2$; average Mn ~5800), tetraethyl-orthosilicate (TEOS, $Si(OC_2H_5)_4$; ≥ 99.0%), toluene (C_7H_8; 99.8 %, ACS), and hexane ($CH_3(CH_2)_4CH_3$; ≥98.5 %; HPLC grade) were obtained from Sigma. Silica-gel, (SiO_2; 0.060–0.2 mm), benzyl alcohol (C_7H_8O; 99+ %, ACS), benzyl benzoate ($C_{14}H_{12}O_2$; 99+ %), benzaldehyde (C_7H_6O; 99 + %), biphenyl ($C_{12}H_{10}$; 99 %), and potassium carbonate (K_2CO_3; 99.0 %, ACS) were obtained from Alfa Aesar. Triethylsilane ($C_6H_{16}Si$; 99%) and sodium borohydride ($NaBH_4$; 99%, Tracemetal) were obtained from ACROS ORGANICS. Nitric acid (HNO_3; 67–70 %, Tracemetal™) was obtained from Fisher Chemical. Platinum−divinyltetramethyldisiloxane complex ($C_{24}H_{54}O_3Pt_2Si_6$; ~2 % Pt in xylene) was obtained from Gelest. Reagent grade water was obtained from Thermo Scientific. Compressed nitrogen gas (N_2, ≥ 99.9 %) and compressed oxygen gas (O_2, ≥ 99.5 %) were supplied by A-L Compressed Gases, INC. Compressed carbon dioxide gas (CO_2, ≥ 99.9 %) was purchased from NorLAB. Carbon/formvar-coated copper TEM grids were purchased from Ted Pella. Toluene was dried over molecular sieves for at least 24 h before usage. The silica-gel was dried in a vacuum oven for 24 h at 150 ℃ before deposition. All other materials were used without any further purification or processing.

2.2. Synthesis of SBA-15

An SBA-15 mesoporous silica was synthesized following a literature procedure [27], and is described in the Supporting Information. The obtained solid materials will be referred to as the "prepared SBA-15 mesoporous silica".

2.3. Synthesis of the molecular liquids and conversion to reversible ionic liquids (RevILs)

The APTES molecular liquid was synthesized following a literature procedure [9], which is described in the Supporting Information. The RevILs are formed by sparging the molecular liquid with CO_2 in a nitrogen-purged vial under magnetic stirring. The mass of the vial was measured every 10 min. Sparging was stopped when no mass change was observed in three consecutive measurements (2 h).

2.4. Synthesis of the reversible ionic liquid (RevIL)-stabilized nanoparticles

The RevIL-stabilized gold nanoparticles were synthesized using a modified method available in the literature [9,10]. $HAuCl_4 0.3\ H_2O$ (0.0298 g; 0.076 mmol) was dissolved in the RevIL (3.7665 g; 0.00943 mmol). 17.6 mL of hexane was added, and the solution was mixed at 600 rpm until the $HAuCl_4$ was completely dissolved. 400 μL of a 0.1 M $NaBH_4$ aqueous solution was added to the vial while stirring. The solution was stirred at 600 rpm for 30 min to completely reduce the gold precursors. The nanoparticles prepared in this manner will be referred to as "colloidal RevIL-stabilized nanoparticles."

2.5. Deposition of the RevIL-stabilized nanoparticles on the non-porous SiO_2

This deposition is followed in a literature procedure [9]; the deposition procedures are presented in the Supporting Information. The prepared materials will be referred to as "Au/SiO_2/A.S.", for gold nanoparticles deposited on non-porous SiO_2 as synthesized.

2.6. Deposition of nanoparticles in the prepared SBA-15 mesoporous silica

The deposition of the RevIL-stabilized gold nanoparticles in SBA-15 mesoporous silica was conducted via an incipient wetness (IW) technique. In a typical deposition, the RevIL-stabilized nanoparticles are first diluted with hexane (1:1—RevIL-stabilized nanoparticles:hexane by volume). The diluted nanoparticle dispersion is then added dropwise to the prepared SBA-15 mesoporous silica with constant mechanical stirring of the solid. The constant stirring ensures that the nanoparticle solution is equally distributed across the SBA-15 mesoporous silica, preventing isolated locations from becoming oversaturated. It takes approximately 40 min to saturate the SBA-15 mesoporous silica fully; the SBA-15 mesoporous silica changes to a pinkish color, implying that the nanoparticles are deposited on the SBA-15 mesoporous silica. The saturated SBA-15 mesoporous silica is left in a loosely capped vial overnight, allowing for complete deposition. The vial is then placed in a vacuum oven until the solid is completely dry the next day. The vacuum oven is regulated at 0.44 atma and 45 °C. The prepared solid materials will be referred to as "Au/SBA-15/A.S." for gold nanoparticles deposited in SBA-15 mesoporous silica, as synthesized. It is noted that adding solution too quickly and without constant stirring often results in the appearance of bulk liquid, indicating that the SBA-15 mesoporous silica is over-saturated. The saturated pores prevent the entrance of nanoparticles, leading to the accumulation of nanoparticles on the external surface of SBA-15 (a failed deposition). It should be noted that it is

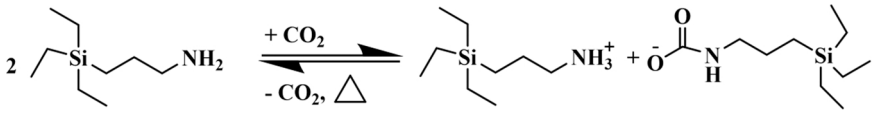

Scheme 1. The reversible reaction of silylamine molecular liquids with CO_2 to form reversible ionic liquids.

possible to increase the gold loading by repeating the deposition process. The efficiency of this deposition method is approximately 96 %, which is comparable to SBA-15 surface-modified methods (~ 99 %) [6].

2.7. Thermal treatment

When indicated, the supported nanoparticles were exposed to a vacuum treatment at 100 °C or a 230 °C calcination at ambient pressure. In the vacuum treatment, 0.03 g of the Au/SBA-15/A.S. preparations were placed in a vacuum oven regulated under 0.44 atma for 24 h at 100 °C. The prepared solid materials are named "Au/SBA-15/100 °C", for the Au/SBA-15/A.S. preparations with an additional 100 °C vacuum calcination. In a typical 230 °C calcination, 0.05 g of Au/SBA-15/A.S. or Au/SiO_2/A.S. preparations were calcined in air using a Thermolyne Benchtop 1100 C Muffle Furnace. The calcination conditions are as follows: the temperature was ramped at 5 °C min^{-1} to 230 °C from the room temperature, held for 180 min, and then allowed to cool to the room temperature. The prepared solid materials are named "Au/SBA-15/230 °C", for the Au/SBA-15/A.S. preparations with additional 230 °C calcination and "Au/SiO_2/230 °C" for the Au/SiO_2 preparations with additional 230 °C calcination.

2.8. Thermogravimetric analysis (TGA)

TGA was performed to measure the mass fraction of the remaining APTES molecular liquids. In a typical TGA experiment, 0.002 mg of the Au/SBA-15/A.S. or the Au/SBA-15/100 °C preparations were placed in a platinum pan attached to a TA Instruments Q50. The TGA conditions are as follows: the temperature was ramped at 5 ℃ min^{-1} to 230 °C from an equilibrium temperature (40 °C), held for 180 min, and then allowed to cool to 40 °C.

2.9. Catalyst characterization

Nanoparticle size was determined using transmission electron microscopy (TEM) utilizing an FEI Technai G2 T20 Twin TEM with an operating voltage of 200 kV. Samples were dispersed in hexane and drop-cast onto a 75-mesh, Cu grid. Image analysis was performed using ImageJ software with at least 200 particles sized.

The nanoparticle gold loadings of catalyst preparations were determined using the Total Reflection X-Ray Fluorescence (TRXF) analysis using a Bruker S4 TSTAR spectrometer. 0.052 g of Au/SBA-15/230 ℃ preparations or 0.054 g of Au/SiO_2/A.S. preparations were dissolved in 1 mL of HNO_3 then submerged in a 40 ℃ water bath for 25 min until no pink color was observed. 40 μL of 1000 mg/L Vanadium (V) (internal standard) in HNO_3 was subsequently added and mixed using vortex-mixer. 10 μL of solution was cast-drop onto a clean quartz disk. The quantification measurement method is as follows: Si (Silicon), Mo (Molybdenum), and Ar (Argon) are assigned as the deconvoluted elements; V (Vanadium) is assigned as the standard element; Au (Gold) is used for quantification. The acquisition is as follows: Mo 17.5 excitation, air, and 1000 s with the "Escape," "Pile up," and "Background" corrections following the profile setting Mo-K.

Attenuated Total Reflectance (ATR) Fourier Transform Infrared Spectroscopy (FTIR) was used to characterize the chemical state of the APTES molecular liquids and RevILs in the catalyst preparations and prepared SBA-15 mesoporous silica utilizing a ThermoScientific Nicolet IS10. The spectra were collected from 650 to 4000 cm^{-1} and scanned 512 times at a resolution of 4 cm^{-1}.

Brunauer-Emmett-Teller (BET) surface area and pore dimension analyses were performed via N_2 adsorption-desorption. A complete isotherm analysis was performed at liquid nitrogen temperature (77 K) using a commercial gas adsorption analyzer (Micromeritics 3Flex). Before the isotherm measurement, the bare SBA-15 mesoporous silica samples (60 mg) were de-gassed in-situ at 150 ℃ at the analysis port for 15 h to remove all the adsorbates from their surface.

2.10. Catalytic activity evaluation

The catalytic activities of all the catalyst preparations were tested in the oxidation of benzyl alcohol. (Scheme 2).

All the reactions were reacted with a base (K_2CO_3) to increase the total rate of reaction. The base (15 mg) and the gold nanoparticle catalysts were added into a 9 mL sealed glass reaction vessel. The total amount of gold was maintained at 0.0559 μmol, accounting for the different mass loadings: 15 mg Au/SBA-15/A.S., 12.3 mg Au/SBA-15/100 ℃, 11.4 mg Au/SBA-15/230 ℃, 16.3 mg Au/SiO_2/A.S., or 14.7 mg Au/SiO_2/230 ℃. Finally, a stock solution of benzyl alcohol (9.6 mmol) and biphenyl (10 μmol, internal standard) was added to the gold catalyst and the base. The glass vial was sealed, sonicated for one minute to mix all species, and then attached to a pressurized O_2 cylinder. The vessel was pressurized to 6 bars of O_2 before venting. The pressurization/venting cycle was repeated three times and allowed to remove all air. Once reduced to atmospheric pressure (~ 99.5 % O_2), the vial was submerged in a 100 ℃ oil bath and magnetically stirred at 600 rpm. After a three-minute thermal equilibration period, the pressure of headspace was raised to 6 bar (> 99.9 % O_2) and the reaction was allowed to react for one hour under 600 rpm stirring. It should be noted that the glass vial was maintained at 6 bar for the duration of the reaction. The reaction was quenched by submerging vials into room temperature water, reduced to atmospheric pressure, and then centrifuged at 6000 rpm for 6 min before taking a 0.5 mL sample for Gas Chromatography with Flame Ionization Detection (GC-FID) analysis. All reactions were performed in triplicate.

GC-FID was conducted using a Thermo Scientific Trace 1310 gas chromograph with an SGE Analytical Science BP5 column (30 m x 0.25 mm x 0.25 μm). A 1.0 μL sample was injected at 300 ℃ under constant pressure mode (25 psi) with a split flow of 90 mL and the following temperature profile: initial temperature 40 ℃, ramp at 7.5 ℃ min^{-1} to 70 ℃, ramp at 15 ℃ min^{-1} to 145 ℃, ramp at 45 ℃ min^{-1} to 280 ℃, and hold for 3 min. The concentrations of all species are determined based upon the calibration curve (Fig. S2) compared to biphenyl internal standard.

3. Results and discussion

To explore the effectiveness of this new nanoparticle deposition technique, we analyzed the location of the nanoparticles (e.g., in the pores of the mesoporous silica vs. on the external surface), studied the impact of the deposition technique on the morphology of nanoparticles, investigated the impacts of various thermal treatment to understand how the reversible ionic liquids' switchable nature is leveraged, and, finally, investigated the impact of the new deposition method on the catalytic activities of the prepared catalysts.

3.1. Physical properties of the prepared SBA-15 mesoporous silica

SBA-15 mesoporous silica was synthesized as the quality of commercial mesoporous silica was not sufficient for fundamental material characterization. We found that the commercial SBA-15 mesoporous silica was difficult to microscopically observe nanoparticles inside pores as there was generally low alignment and there were large amorphous regions. The surface area and average pore diameter of the prepared SBA-15 mesoporous silica was determined via an N_2 adsorption-desorption isotherm (Fig. S3). The average pore diameter and surface areas are as follows: 6.63 nm, 665 m^2/g (macro), and 152 m^2/g (micro).

3.2. Determination of the location of the nanoparticles in the Au/SBA-15/A.S. preparations

We needed to confirm that this RevIL deposition technique was able to deposit nanoparticles in the pores of SBA-15 mesoporous silica and not only on the external surface of SBA-15. Fig. 1A is a TEM micrograph

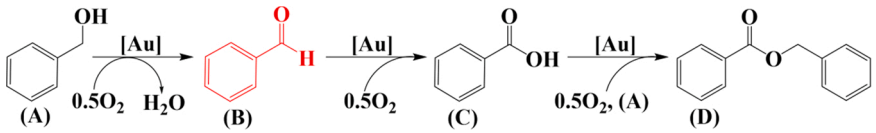

Scheme 2. Gold-catalyzed sequential oxidation of (A) benzyl alcohol into (B) benzaldehyde, (C) benzoic acid, and (D) benzyl benzoate.

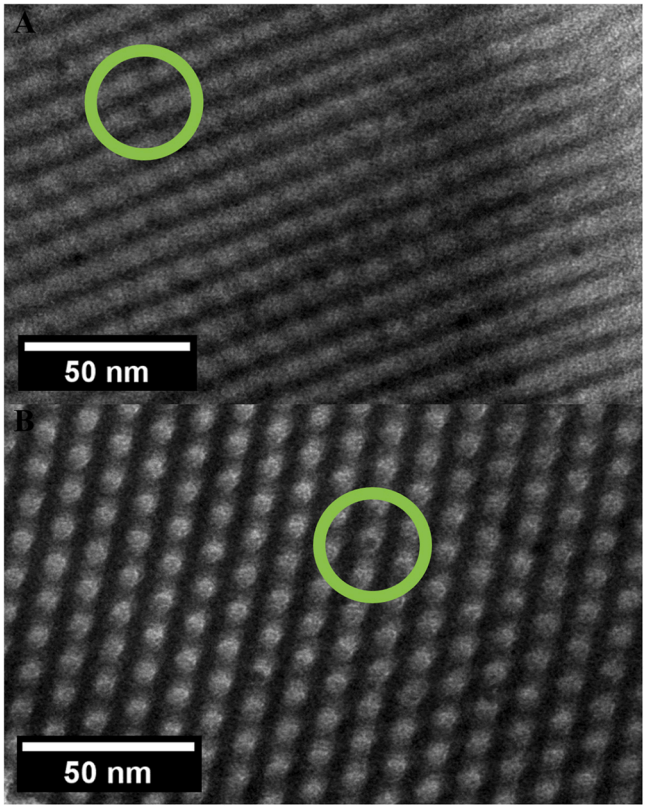

Fig. 1. The TEM micrographs of the Au/SBA-15/A.S. preparations. (B) was obtained by rotating (A) to +20 degrees.

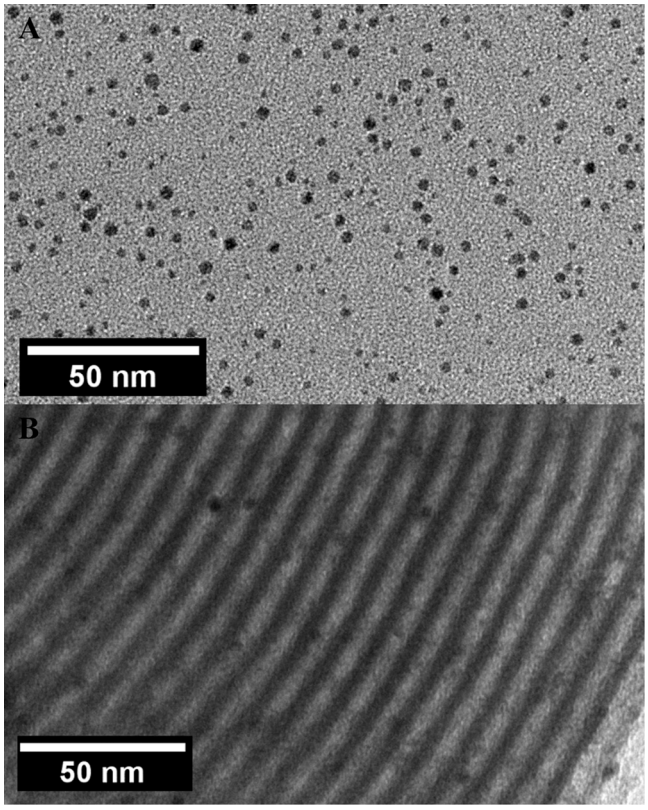

Fig. 2. The representative TEM micrographs of (A) colloidal RevIL-stabilized nanoparticles, and (B) Au/SBA-15/A.S. preparations.

showing the nanoparticles aligning with the channels of mesoporous silica. However, simply demonstrating the alignment of nanoparticles with the channel is insufficient to conclude that nanoparticles are inside the pores (e.g., they could be on the external surface of the SBA-15 mesoporous silica). By tilting the TEM platform, we confirm that the observed nanoparticles that align with the channels are inside the pores by then observing the same nanoparticles from a different perspective. The TEM platform was then rotated to +20 degrees to obtain Fig. 1B. Fig. 1B shows that the nanoparticles aligned with the channels in Fig. 1A are in the interior of the pore. This confirms that we can use this RevIL deposition technique to easily deposit nanoparticles in the pores of SBA-15 mesoporous silica without the needs for functionalizing the SBA-15 surface.

3.3. Effect of deposition on nanoparticle size

After confirming that this RevIL deposition technique can deposit nanoparticles in the pores of SBA-15 mesoporous silica, we need to confirm, similar to our prior experience [9], that this RevIL technique is able to maintain the nanoparticle size throughout the deposition, providing a level of size control. Fig. 2A is a TEM micrograph of the colloidal RevIL-stabilized nanoparticles with 3.46 ± 0.53 nm average diameter (Table 1). The histograms of all nanoparticle size distributions are available in the Supporting Information. Fig. 2B is a representative TEM micrograph of the Au/SBA-15/A.S. preparations used for nanoparticle sizing. The gold nanoparticles in the Au/SBA-15/A.S. preparations were determined to be 3.28 ± 0.42 nm average diameter. There was no significant statistical change (determined by a single-factor ANOVA analysis and Tukey HSD [28] with $p > 0.05$ in all cases) in the particle size from the colloidal RevIL-stabilized gold nanoparticles to the Au/SBA-15/A.S. preparations. The ANOVA analysis is presented in the Supporting Information. Hence, we can conclude that this RevIL deposition technique is able to maintain the nanoparticle size

Table 1
Nanoparticle size, gold loading, and number of gold surface atoms/g catalyst for all catalyst preparations. All nanoparticle size distributions are available in the Supporting Information.

Catalyst sample naming	Average nanoparticle diameter (nm)	Gold loading (mg Au/ g catalyst)	Au surface atoms/g catalysts x 10^{18}
Colloidal nanoparticles	3.46 ± 0.53		
Au/SBA-15/A.S.	3.28 ± 0.42	0.734	0.754
Au/SBA-15/ 100 °C	3.48 ± 0.58	0.898	0.847
Au/SBA-15/ 230 °C	3.65 ± 0.57	0.966	0.868
Au/SiO_2/A.S.	2.62 ± 0.75	0.678	0.753
Au/SiO_2/230 °C	7.41 ± 3.02	0.753	0.277

throughout deposition.

3.4. ATR-FTIR analysis

The ATR-FTIR spectrums of APTES molecular liquids, RevILs, colloidal nanoparticles, catalyst preparations, and prepared SBA-15 mesoporous silica are shown in Fig. 3. The APTES molecular liquids are identifiable by the CH_2 peaks at 2900 cm^{-1} and the N-H stretching of amine at 3250–3370 cm^{-1} [29]. The CH_2 peaks are seen again in the RevIL spectrum as the reaction of APTES molecular liquids with CO_2 forms RevILs. The RevILs are characterized by the asymmetric NCO_2^- stretch of the carbamate ion at 1575 cm^{-1} [29]. The colloidal nanoparticles are only stabilized by RevILs as the N-H stretching of amine is absent. The absence of the asymmetric NCO_2^- stretch of the carbamate ion, and the presence of the CH_2 peaks are observed in the Au/SBA-15/A.S. spectrum, suggesting that vacuum-oven drying was sufficient to reverse the RevILs to the APTES molecular liquids. The full-scale NCO_2^- and N-H stretches are shown in Fig. S7 (A) and (B), respectively. It should be noted that the peak towards 1650 cm^{-1} for the Au/SBA-15/A.S., Au/SBA-15/100 ℃, and prepared SBA-15 is likely ascribed to the adsorbed water [30] and does not belong to carbamate ions. Furthermore, the N-H stretching of amine (3250–3370 cm^{-1}) is observed in the Au/SBA-15/A.S. spectrum. This implies that at least some APTES molecular liquids do not bind with gold nanoparticles as the N-H stretch of amine should disappear when amines interact with gold nanoparticles [31]. However, we cannot exclude the possibility that some APTES molecular liquids bind to the gold nanoparticles. Previous analysis [10] using x-ray photoelectron spectroscopy (XPS) has concluded that these reversal conditions result in the gold surface being effectively bare without any APTES molecular liquids. Comparatively, the N-H stretch of molecular liquids was not observed in the Au/SBA-15/100 °C spectrum. In comparing the 3100–3500 cm^{-1} regions in the prepared SBA-15 and the Au/SBA-15/100 °C spectrums, we see a broad water peak. This broad water peak overlaps with the N-H stretching of amine, leading to the underrepresentation of the intensity of the N-H stretching of the amine in the Au/SBA-15/100 °C spectrum. In summary, the FTIR results indicate that the incipient wetness RevIL catalyst synthesis technique is sufficient to completely reverse RevILs to APTES molecular liquids, and if this is in an agreement with previous results, should be catalytically active. Additionally, the further reduction of the molecular liquids during low-temperature calcination should further increase catalytic activity due to greater surface accessibility.

3.5. Calcination experiments

One major benefit of catalyst designs leveraging nanoparticles inside the pores of mesoporous silica is the improved thermal stability. Furthermore, it has been demonstrated that RevIL-prepared catalysts reduce the sintering of nanoparticles during calcination compared to traditionally prepared thiol-stabilized nanoparticles [10]. The calcination experiments are used to determine if leveraging the pore structure of SBA-15 would improve the thermal stability, resulting in less change in nanoparticle size.

As a control, the Au/SiO_2/A.S. preparations (Fig. 4A) can be compared to the Au/SiO_2/230 °C preparations (Fig. 4B) to investigate the expected degree of nanoparticle sintering in the absence of a pore environment. The Au/SiO_2/230 °C preparations show much larger nanoparticles than the Au/SiO_2/A.S. preparations where the calcination

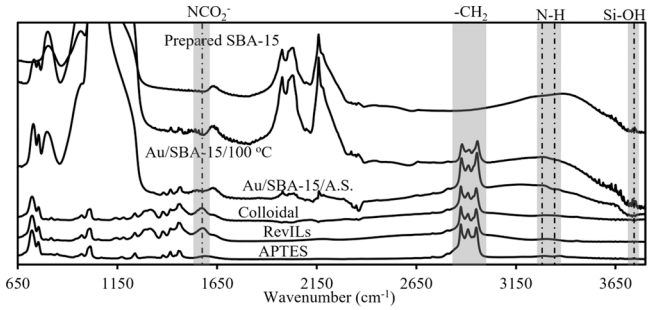

Fig. 3. ATR-FTIR spectra of all the synthesis components, catalyst preparations, and prepared SBA-15 mesoporous silica. Note: Au/SBA-15/100 °C and Prepared SBA-15 are shown at a greater magnification to show greater detail.

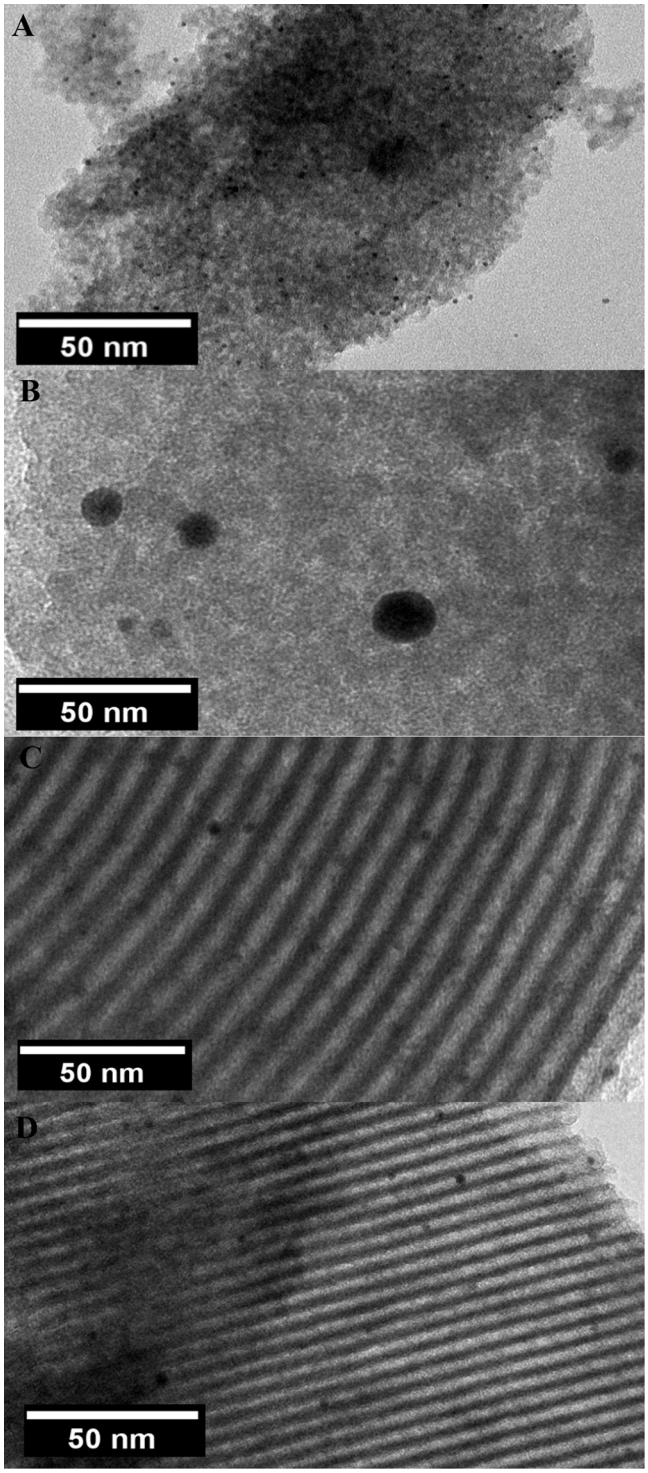

Fig. 4. The representative TEM micrographs of (A) Au/SiO_2/A.S. preparations, (B) Au/SiO_2/230 °C preparations, (C) Au/SBA-15/A.S. preparations, and (D) Au/SBA-15/230 °C preparations.

leads to a 183 % (7.41 ± 3.02 nm vs. 2.62 ± 0.75 nm) increase in the average diameter of Au/SiO_2/230 °C preparations (Table 1). Previous work indicated that the RevIL promotes sinter-resistance compared to traditionally prepared thiol-stabilized nanoparticles exposed to the same calcination [10]. The growth of these nanoparticles likely proceed via a particle migration and coalescence and/or Ostwald Ripening mechanism during calcination [32,33]; therefore, the sintering of the gold nanoparticles in the SiO_2 preparations is thermodynamically favorable. Comparatively, no practical nanoparticle morphology changes were observed between the Au/SBA-15/A.S. preparations (Fig. 5C) and the Au/SBA-15/230 °C preparations (Fig. 5D). The calcination results in an 11.3 % (3.65 ± 0.57 nm vs. 3.28 ± 0.42 nm) increase in the average diameter of the Au/SBA-15/230 °C preparations (Table 1). This indicates that the pore structure of SBA-15 improves the nanoparticles' thermal stability under calcination conditions compared to the non-porous SiO_2, thus providing an additional confirmation that the nanoparticles are inside the pores of SBA-15. Furthermore, Fig. 5C shows that the nanoparticles are far from each other as they are geometrically separated by the pores—the SBA-15 pore structure has created the additional energy barriers for inhibiting the sintering rate of nanoparticles [13,34,35]. These results agree with literature—the gold catalysts supported by mesoporous material have superior thermal stability compared to those prepared on high surface metal oxide supports [13,36,37].

3.6. Catalytic activity evaluation

The catalytic activities of all the catalyst preparations were evaluated in the oxidation of benzyl alcohol. This reaction has been used as a popular model catalytic test due to simple setup and handling procedures and relatively mild reaction conditions [38–40]. More importantly, this reaction is a benchmark to assess the activities of gold catalysts for promoting selective oxidation of benzyl alcohol [41].

The conversion of benzyl alcohols and the selectivity and yield of benzaldehyde and benzyl benzoate are reported as percentages and defined in Eqs. (1–4):

$$X = \frac{n_{BnOH\_I} - n_{BnOH}}{n_{BnOH\_I}} \quad (1)$$

$$S_{BnCHO} = \frac{n_{BnCHO}}{n_{BnOCO} + n_{BnCHO}} \quad (2)$$

$$S_{BnOCO} = \frac{n_{BnOCO}}{n_{BnOCO} + n_{BnCHO}} \quad (3)$$

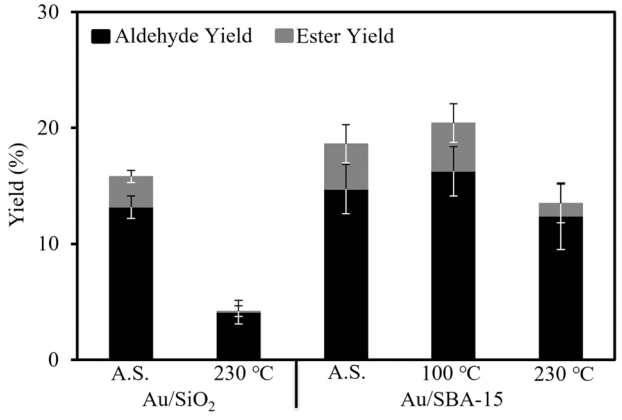

Fig. 5. The product yields using the Au/SiO_2/A.S., Au/SiO_2/230 °C, Au/SBA-15/A.S., Au/SBA-15/100 °C, and Au/SBA-15/230 °C preparations. Reaction conditions: gold loadings of all catalyst preparations were maintained at 0.0559 μmol, 15 mg of K_2CO_3 for all reactions, 99.9 % O_2, 1 h, 600 rpm, 100 °C.

$$Y_i = X \cdot S_i \quad (4)$$

Where X is the conversion of benzyl alcohol, n_{BnOH} is the number of moles of benzyl alcohol at the conclusion of the reaction, n_{BnOH_I} is the initial number of moles of benzyl alcohol, S_{BnCHO} is the selectivity towards benzaldehyde, n_{BnCHO} is the number of moles of benzaldehyde after the reaction, n_{BnOCO} is the number of moles of benzyl benzoate after the reaction, S_{BnOCO} is the selectivity towards benzyl benzoate, and Y is the yield of benzaldehyde or benzyl benzoate. Furthermore, the sum of the yields of benzaldehyde and benzyl benzoate is considered as the conversion of benzyl alcohol as the overall mass balance is less than 5 % different from the stock solution.

The molar turnover frequency (TOF_M) is shown in Table 2 and defined as:

$$TOF_M = \frac{n_{BnOH}}{n_{Au} \cdot t} \quad (5)$$

Where n_{Au} is the total moles of gold that were determined based on the TRXF and TGA results, and t is the time of reaction. A TOF_M value is often reported as a "turnover frequency" in the literature [42–44], making it a useful comparison when the nanoparticle size is similar [45]. However, such comparison is not normalized based upon the active sites.

To compare the fundamental catalysis, the turnover frequency on the surface atom basis was calculated for each catalyst preparation (Table 2). A surface turnover frequency (TOF_S) is defined in Eq. 6:

$$TOF_S = \frac{n_{BnOH}}{n_{Au_{Surface}} \cdot t} \quad (6)$$

Where $n_{Au_{Surface}}$ represents the number of moles of gold surface atoms across the total surface area of the active phase in a given reaction. The surface gold atoms are calculated geometrically based upon gold loading (determined by the TRXF and TGA results), average nanoparticle size, and population polydispersity (Table 1). A demonstration of such calculation can be found in the Surface Atom Calcination Method section of the Supporting Information.

3.7. The catalytic activities of the Au/SBA-15/A.S. and the Au/SBA-15/100 °C preparations

It should be noted that the selective oxidation of benzyl alcohol does not proceed in the absence of catalyst. The benzyl alcohol conversions using the Au/SBA-15/A.S. and Au/SBA-15/100 °C preparations are shown in Fig. 5. The Au/SBA-15/A.S. preparations show an 18.6 % conversion and 79.0 % selectivity toward benzaldehyde. The Au/SBA-15/A.S. preparations are catalytically active, indicating that calcination is not needed to remove the ligands from the gold surface, in agreement with the FTIR results. Additionally, they show a statistically significant decrease in the conversion (determined by a single-factor ANOVA analysis and Tukey HSD [28] with $p < 0.05$ in all cases, except cycle 3 vs. cycle 4) during four consecutive cycles, where cycle 1 is statistically significant from cycles 2–4; cycle 2 is statistically significant from cycles 3–4, which do not show a statistical significance. The ANOVA statistical analysis is presented in the Supporting Information. The conversion reduces in cycles 1–2, from 18.0 % to 9.80 % (approximately 53.5 % of initial conversion), and then remains roughly constant

Table 2
A molar and surface turnover frequency of each catalyst preparation in the selective oxidation of benzyl alcohol.

Catalyst sample	TOF_M (s^{-1})	TOF_S (s^{-1})
Au/SBA-15/A.S.	8.89	26.4
Au/SBA-15/100 °C	9.75	31.5
Au/SBA-15/230 °C	6.44	21.9
Au/SiO_2/A.S.	7.54	20.7
Au/SiO_2/230 °C	2.00	16.5

for the subsequent consecutive runs (Fig. S9). The apparent decrease in the conversion can be explained by the reaction-induced growth of nanoparticles as a 56 % increase (3.28 ± 0.42 nm to 5.12 ± 0.92 nm) in the particle size is observed during the reaction (Fig. S6). While there are practical impacts that reduce the conversion, the fundamental measurement of activity (TOF_S) indicates that the activity remains relatively constant from cycle 1 ($TOF_S = 25.5\ s^{-1}$) to cycle 2 ($TOF_S = 22.2\ s^{-1}$). Comparatively, the Au/SBA-15/100 °C preparations show an increase in conversion (20.4 %) without sacrificing the selectivity toward benzaldehyde (79.5 %). Additionally, the TOF values of the Au/SBA-15/100 °C preparations ($TOF_M = 9.75\ s^{-1}$, $TOF_S = 31.5\ s^{-1}$) are higher than that of the Au/SBA-15/A.S. preparations ($TOF_M = 8.89\ s^{-1}$, $TOF_S = 26.4\ s^{-1}$). These differences in TOF values can be explained due to the presence of some APTES molecular liquids remaining on the catalyst's surface. The FTIR results (Fig. 3) have demonstrated the presence of APTES molecules on the catalyst surface; however, FTIR cannot distinguish if they are chemisorbed to the gold surface, are chemisorbed to the SBA-15 silica, or are physisorbed to the catalyst surface. Furthermore, a previous work [10] using XPS has demonstrated that the APTES molecular liquids are not chemisorbed to the gold surface but are chemisorbed to the non-porous silica. However, this XPS result cannot eliminate the possibility that some APTES molecular liquids are physisorbed to the gold surface to block sites, thus reducing the number of active sites. The TGA results show a 250 % greater mass loss for the Au/SBA-15/A.S. preparations than the Au/SBA-15/100 °C preparations, indicating that a 100 ℃-calcination is sufficient to remove the APTES molecular liquids and effectively increases the total number of surface sites. The TGA results are shown in Fig. S8. Since the surface area used in the TOF calculation is a geometric determination and not a measurement, we are likely overestimating the number of sites for the Au/SBA-15/A.S. preparation, thus decreasing the true TOF value. Therefore, the number of sites and TOF value for the Au/SBA-15/100 ℃ preparation are more accurate.

3.8. The activities of the non-porous and porous gold catalysts before and after a 230 °C calcination

The catalytic activities of the Au/SiO_2/A.S. preparations and the Au/SBA-15/A.S. preparations are compared to investigate the impacts of pore and non-pore environments on the catalytic activities. The catalytic activities of the Au/SBA-15/230 °C preparations and the Au/SiO_2/230 °C are compared to investigate the impact of particle size on the catalytic activities.

The conversion using the Au/SiO_2/A.S., Au/SiO_2/230 ℃, Au/SBA-15/A.S., and Au/SBA-15/230 ℃ preparations are shown in Fig. 5. The Au/SiO_2/A.S. preparations show a 15.8 % conversion and 83.3 % selectivity toward benzaldehyde. Comparatively, the Au/SBA-15/A.S. preparations show a higher conversion (18.6 %) and a 79.0 % selectivity toward benzaldehyde. Furthermore, the TOF values of the Au/SBA-15/A.S. preparations ($TOF_M = 8.89\ s^{-1}$, $TOF_S = 26.4\ s^{-1}$) are higher than that of the Au/SiO_2/A.S. preparations ($TOF_M = 7.54\ s^{-1}$, $TOF_S = 20.7\ s^{-1}$), implying that there is an improved fundamental catalytic-activity after correcting for any impacts of loading or differences in the number of surface sites. Since the gold surface is effectively the same, all the other impacts must be due to the SBA-15 pore environment. Furthermore, the data is practically and statistically significant for activity analysis (determined by a single-factor ANOVA analysis and Tukey HSD [28] with $p < 0.05$ in all cases). The ANOVA statistical analysis is presented in the Supporting Information. Hence, the improved activity and the statistical significance in the data support the enhancement of catalytic activity induced by the SBA-15 pore geometry. The Au/SiO_2/230 °C preparations show only a 4.20 % conversion and 98.0 % selectivity toward benzaldehydes; the increase (98.0 % vs. 83.3 %) in the benzaldehyde's selectivity (compared to the Au/SiO_2/A.S. preparations) is consistent with this. The nature of thermodynamically favorable reactions in series inherently leads to an increase in selectivity towards the intermediate products at lower conversions [45]. Additionally, the TOF values of the Au/SiO_2/230 ℃ preparations ($TOF_M = 2.00\ s^{-1}$, $TOF_S = 16.5\ s^{-1}$) are significantly smaller than that of the Au/SiO_2/A.S. preparations ($TOF_M = 7.54\ s^{-1}$, $TOF_S = 20.7\ s^{-1}$), implying the significant reduction in the activities of the non-porous gold catalysts after a 230 ℃ calcination. Such dramatic reduction in the activities can be attributed to a particle size effect (183 % increase in the particle size after a 230 ℃ calcination) in which the larger nanoparticles are fundamentally less active, likely due to significant reductions in the true active sites [46]. Comparatively, the Au/SBA-15/230 °C preparations show a 13.5 % conversion and 91.8 % selectivity toward benzaldehydes. Compared to the Au/SBA-15/A.S. preparations, the TOF values of Au/SBA-15/230 °C preparations ($TOF_M = 6.44\ s^{-1}$, $TOF_S = 21.9\ s^{-1}$) were slightly reduced; however, they are still as active as the Au/SiO_2/A.S. preparations ($TOF_M = 7.54\ s^{-1}$, $TOF_S = 20.7\ s^{-1}$) and are significantly more active than the Au/SiO_2/230 °C preparations ($TOF_M = 2.00\ s^{-1}$, $TOF_S = 16.5\ s^{-1}$).

4. Conclusion

We have demonstrated that without the needs of the SBA-15 surface functionalization, the RevIL catalyst synthesis technique can deposit the RevIL-stabilized gold nanoparticles inside the pores of the SBA-15 mesoporous silica. The nanoparticles inside the SBA-15 pores show improved thermal stability under a 230 ℃ calcination compared to those supported on the surface of non-porous SiO_2. Nanoparticles sintered on the surface of the non-porous SiO_2, where the sintering was evidenced by TEM images and a 183 % increase in particle size. As the FTIR results indicated, vacuum-oven drying has completely reversed the RevILs to the APTES molecular liquids. Hence, the as-synthesized porous gold catalysts are active in the selective oxidation of benzyl alcohol without calcination. Additionally, they are more active than the as-synthesized non-porous gold catalysts, indicating that the pore geometry enhances catalytic activities. Furthermore, catalysts' activities were improved following a 100 ℃ calcination, which is significantly milder than a 500 ℃-calcination benchmark. Up to a 230 ℃ calcination, the calcined porous gold catalysts are as active as the as-synthesized non-porous gold catalysts and are significantly more active than the calcined non-porous gold catalysts. The significant reduction in the activities of the calcined non-porous gold catalysts is likely due to the particle size effect (an 183 % increase in particle size). Lastly, the perceived benefits of this RevIL catalyst synthesis technique and the catalytic performance of the gold catalysts prepared by the RevIL technique are summarized. The RevIL technique is able to deposit gold nanoparticles in the pores of SBA-15 mesoporous silica, evidenced by the representative TEM images (Fig. 1) and the measured increase in the thermal stability from the porous SBA-15 silica to the non-porous silica. Additionally, the RevIL technique has effectively eliminated the needs for passivating the catalyst surface, potentially leading to more advanced catalyst structures that leverage triple-phase boundaries or strong metal-support interactions (SMSI), allowing for this technique to be translated to other types of mesoporous supports with minimal effort. Furthermore, the RevIL technique is able to provide a fine control over the nanoparticle size during deposition, agreeing with our previous results [9]. The as-synthesized gold catalysts prepared by the RevIL technique do not require calcination for catalysis, as they are immediately active in the selective oxidation of benzyl alcohol reaction due to the bare surface sites after deposition [10]. Additionally, the porous SBA-15 supported gold catalysts show a statistically significant increase in activity compared to the non-porous silica supported gold catalysts, implying that the pore geometry enhances catalytic performance. Furthermore, their activity does increase after a low-temperature (e.g., 100 ℃) calcination treatment—likely due to the removal of unbounded APTES molecular liquids; it should be noted that a 100 ℃-calcination is significantly milder than the 500 ℃-benchmark calcination.

CRediT authorship contribution statement

Zengran Sun: Methodology, Validation, Formal analysis, Investigation, Data curation, Writing – original draft, Writing – review & editing, Visualization. **Ellis Hammond-Pereira:** Formal analysis, Writing – review & editing. **Xianghui Zhang:** Investigation, Validation, Formal analysis, Writing – review & editing. **Di Wu:** Resources, Writing – review & editing. **Steven R. Saunders:** Conceptualization, Writing – review & editing, Supervision, Project administration, Funding acquisition.

Declaration of Competing Interest

The authors declare that they have no known competing financial interests or personal relationships that could have appeared to influence the work reported in this paper.

Acknowledgement

This work was supported by the National Science Foundation, USA under grant CAREER-1651597. The authors acknowledge the institutional funds from the Gene and Linda Voiland School of Chemical Engineering and Bioengineering and Alexandra Navrotsky Institute for Experimental Thermodynamics at Washington State University, USA. The authors thank the Franceschi Microscopy & Imaging Center and the Nuclear Magnetic Resonance Center to make the material characterization studies become possible. The authors thank Dr. Nobert Kruse's generosity and Rui Zhang's assistance on muffle furnace. The material synthesis of APTES, RevILs, and non-porous gold catalysts was completed with the assistance of Dr. Kristin Bryant.

Appendix A. Supporting information

Supplementary data associated with this article can be found in the online version at doi:10.1016/j.apcata.2022.118725.

References

[1] M. Shamzhy, M. Opanasenko, P. Concepción, A. Martínez, Chem. Soc. Rev. 48 (4) (2019) 1095–1149, https://doi.org/10.1039/c8cs00887f.
[2] J.E. Mondloch, E. Bayram, R.G. Finke, J. Mol. Catal. A Chem. 355 (2012) 1–38, https://doi.org/10.1016/j.molcata.2011.11.011.
[3] J. Hu, L. Chen, K. Zhu, A. Suchopar, R. Richards, Catal. Today 122 (3–4) (2007) 277–283, https://doi.org/10.1016/j.cattod.2007.01.012.
[4] H. Song, R.M. Rioux, J.D. Hoefelmeyer, R. Komor, K. Niesz, M. Grass, P. Yang, G. A. Somorjai, J. Am. Chem. Soc. 128 (9) (2006) 3027–3037, https://doi.org/10.1021/ja057383r.
[5] L.F. Gutiérrez, S. Hamoudi, K. Belkacemi, Catalysts (2011), https://doi.org/10.3390/catal1010097.
[6] C.Y. Ma, B.J. Dou, J.J. Li, J. Cheng, Q. Hu, Z.P. Hao, S.Z. Qiao, Appl. Catal. B Environ. 92 (1–2) (2009) 202–208, https://doi.org/10.1016/j.apcatb.2009.07.007.
[7] A. Kumar, B. Sreedhar, K.V.R. Chary, J. Nanosci. Nanotechnol. 15 (2) (2015) 1714–1724, https://doi.org/10.1166/jnn.2015.9022.
[8] X. Chu, C. Wang, L. Guo, Y. Chi, X. Gao, X. Yang, J. Chem. 2015 (2015), https://doi.org/10.1155/2015/737921.
[9] K. Bryant, G. Ibrahim, S.R. Saunders, Langmuir (2017), https://doi.org/10.1021/acs.langmuir.7b02983.
[10] K. Bryant, C.W. West, S.R. Saunders, Appl. Catal. A Gen. 579 (February) (2019) 58–64, https://doi.org/10.1016/j.apcata.2019.04.016.
[11] K. Bryant, E. Hammond-Pereira, S.R. Saunders, J. Phys. Chem. B (2021), https://doi.org/10.1021/acs.jpcb.0c08908.
[12] Y.Q. Su, J.X. Liu, I.A.W. Filot, E.J.M. Hensen, Chem. Mater. 29 (21) (2017) 9456–9462, https://doi.org/10.1021/acs.chemmater.7b03555.
[13] M. Sankar, Q. He, R.V. Engel, M.A. Sainna, A.J. Logsdail, A. Roldan, D.J. Willock, N. Agarwal, C.J. Kiely, G.J. Hutchings, Chem. Rev. (2020), https://doi.org/10.1021/acs.chemrev.9b00662.
[14] Y. Zhu, D. Wang, L. Zhang, F. Sun, J. Xu, S. Jiang, Q. Yu, RSC Adv. (2013), https://doi.org/10.1039/c3ra41338a.
[15] W.R. Glomm, G. Øye, J. Walmsley, J. Sjöblom, J. Dispers. Sci. Technol. 26 (6) (2005) 729–744, https://doi.org/10.1081/DIS-200063041.
[16] F. Xie, Z. Xie, P. Liu, Y. Yuan, J. Li, S. Chen, F. Guo, J. Chen, Z. Gu, Microporous Mesoporous Mater. 266 (March) (2018) 177–182, https://doi.org/10.1016/j.micromeso.2018.03.001.
[17] A.S. Maria Chong, X.S. Zhao, J. Phys. Chem. B 107 (46) (2003) 12650–12657, https://doi.org/10.1021/jp035877.
[18] J. Zhao, H. Yuan, X. Qin, K. Tian, Y. Liu, C. Wei, Z. Zhang, L. Zhou, S. Fang, Catal. Lett. (2020), https://doi.org/10.1007/s10562-020-03190-3.
[19] J. Bouchet, G. Rochat, Y. Leterrier, J.A.E. Månson, P. Fayet, Surf. Coat. Technol. 200 (14–15) (2006) 4305–4311, https://doi.org/10.1016/j.surfcoat.2005.02.148.
[20] X.S. Zhao, G.Q. Lu, J. Phys. Chem. B 102 (9) (1998) 1556–1561, https://doi.org/10.1021/jp972788m.
[21] L. Mercier, T.J. Pinnavaia, Chem. Mater. 12 (1) (2000) 188–196, https://doi.org/10.1021/cm990532i.
[22] P. Mohapatra, S. Shaw, D. Mendivelso-Perez, J.M. Bobbitt, T.F. Silva, F. Naab, B. Yuan, X. Tian, E.A. Smith, L. Cademartiri, Nat. Commun. 8 (1) (2017), https://doi.org/10.1038/s41467-017-02267-9.
[23] M. Haruta, CATTECH (2002), https://doi.org/10.1023/A:1020181423055.
[24] M. Shepida, O. Kuntyi, S. Nichkalo, G. Zozulya, S. Korniy, Adv. Mater. Sci. Eng. (2019), https://doi.org/10.1155/2019/2629464.
[25] C. Louis, Catalysts (2016), https://doi.org/10.3390/catal6080110.
[26] A.S. Sharma, H. Kaur, D. Shah, RSC Adv. (2016), https://doi.org/10.1039/c5ra25646a.
[27] E.M. Björk, J. Chem. Educ. 94 (1) (2017) 91–94, https://doi.org/10.1021/acs.jchemed.5b01033.
[28] J. Vierheller, Commun. Comput. Inf. Sci. 500 (2014) 110–126, https://doi.org/10.1007/978-3-662-45006-2_9.
[29] J.R. Switzer, A.L. Ethier, K.M. Flack, E.J. Biddinger, L. Gelbaum, P. Pollet, C. A. Eckert, C.L. Liotta, Ind. Eng. Chem. Res. (2013), https://doi.org/10.1021/ie4018836.
[30] N. Mittal, A. Samanta, P. Sarkar, R. Gupta, Energy Sci. Eng. 3 (3) (2015) 207–220, https://doi.org/10.1002/ese3.64.
[31] G. Yang, W.S. Chang, D.T. Hallinan, J. Colloid Interface Sci. 460 (2015) 164–172, https://doi.org/10.1016/j.jcis.2015.08.054.
[32] T.W. Hansen, A.T. Delariva, S.R. Challa, A.K. Datye, Acc. Chem. Res. 46 (8) (2013) 1720–1730, https://doi.org/10.1021/ar3002427.
[33] M.T. Bore, H.N. Pham, E.E. Switzer, T.L. Ward, A. Fukuoka, A.K. Datye, J. Phys. Chem. B (2005), https://doi.org/10.1021/jp045917p.
[34] N. Liu, G. Chen, W. Dong, C. Liu, C. Xu, Gold Bull. 50 (2) (2017) 163–175, https://doi.org/10.1007/s13404-017-0206-z.
[35] J. Chen, R. Zhang, L. Han, B. Tu, D. Zhao, Nano Res. 6 (12) (2013) 871–879, https://doi.org/10.1007/s12274-013-0363-1.
[36] J. Liu, Q. Ji, T. Imai, K. Ariga, H. Abe, Sci. Rep. (2017), https://doi.org/10.1038/srep41773.
[37] C.J. Gommes, Nanoscale (2019), https://doi.org/10.1039/c9nr01349k.
[38] V.R. Choudhary, A. Dhar, P. Jana, R. Jha, B.S. Uphade, Green Chem. 7 (11) (2005) 768–770, https://doi.org/10.1039/b509003b.
[39] V.R. Choudhary, R. Jha, P. Jana, Green Chem. 9 (3) (2007) 267–272, https://doi.org/10.1039/b608304h.
[40] R.H. Adnan, G.G. Andersson, M.I.J. Polson, G.F. Metha, V.B. Golovko, Catal. Sci. Technol. 5 (2) (2015) 1323–1333, https://doi.org/10.1039/c4cy01168f.
[41] C.Y. Ma, J. Cheng, H.L. Wang, Q. Hu, H. Tian, C. He, Z.P. Hao, Catal. Today 158 (3–4) (2010) 246–251, https://doi.org/10.1016/j.cattod.2010.03.080.
[42] C.P. Ferraz, M.A.S. Garcia, É. Teixeira-Neto, L.M. Rossi, RSC Adv. 6 (30) (2016) 25279–25285, https://doi.org/10.1039/c6ra01795a.
[43] S.A.C. Carabineiro, Front. Chem. (2019), https://doi.org/10.3389/fchem.2019.00702.
[44] P. Miedziak, M. Sankar, N. Dimitratos, J.A. Lopez-Sanchez, A.F. Carley, D. W. Knight, S.H. Taylor, C.J. Kiely, G.J. Hutchings, Catal. Today 164 (1) (2011) 315–319, https://doi.org/10.1016/j.cattod.2010.10.028.
[45] E. Hammond-Pereira, K. Bryant, T.R. Graham, C. Yang, S. Mergelsberg, D. Wu, S. R. Saunders, React. Chem. Eng. 5 (10) (2020) 1939–1949, https://doi.org/10.1039/d0re00198h.
[46] P. Suchomel, L. Kvitek, R. Prucek, A. Panacek, A. Halder, S. Vajda, R. Zboril, Sci. Rep. (2018), https://doi.org/10.1038/s41598-018-22976-5.